Prospects of emerging polymer-stabilized blue-phase liquid-crystal displays

Linghui Rao
Jin Yan
Shin-Tson Wu

Abstract — The prospects of emerging polymer-stabilized blue-phase liquid-crystal displays, or more generally, Kerr-effect-induced isotropic-to-anisotropic transition, are analyzed with special emphases on the temperature effects. As the temperature increases, both the Kerr constant, induced birefringence, and response time decrease but at different rates. The proposed physical models fit well with experimental results. Some remaining technical challenges associated with this promising display technology are discussed.

Keywords — *Blue-phase liquid crystal, Kerr effect, fast response time.*
DOI # 10.1889/JSID18.11.1

1 Introduction

Fast response time not only reduces the undesirable motion-picture image blur but also enables color-sequential liquid-crystal displays (LCDs) using RGB (red, green, blue) LED backlights.[1,2] The latter is particularly attractive because it eliminates spatial color filters which in turn triples the optical efficiency and resolution density. Higher optical efficiency leads to lower power consumption which implies to an energy saving and longer battery life. However, in order to minimize color breakup in color-sequential displays, the LC response time should be less than ~1 msec which imposes a big challenge to nematic LCDs.[3,4] Various approaches for reducing LC response time have been developed, such as thin cell gap,[5,6] overdrive and undershoot voltage,[7,8] bend cell,[9–11] and low-viscosity LC materials.[12] However, the state-of-the-art LC response time is about 2–3 msec. There is an urgent need to develop LCDs with submillisecond response time.

Recently, polymer-stabilized blue-phase liquid crystal (BPLC)[13–16] is emerging with potential to become a next-generation display because it exhibits the following revolutionary features: (1) submillisecond gray-to-gray response time,[17] (2) no need for surface alignment layer, (3) wide and symmetric viewing angle, and (4) cell-gap insensitivity provided that an in-plane-switching (IPS) electrode is employed.[18] The operation mechanism of a polymer-stabilized blue-phase liquid-crystal display (BPLCD) is drastically different from conventional nematic LCDs; the former is based on the Kerr-effect-induced isotropic-to-anisotropic transition[19] while the latter relies on the anisotropic-to-anisotropic LC director reorientation. Extensive efforts on developing new BPLC materials and low-voltage device structures have been recently performed.[20–24] However, very few experimental results and physical models for understanding the temperature effects on the Kerr constant and response time have been published.[25]

In this paper, we first give a brief review on the underlying Kerr effect and then report on a systematic study on how operating temperature affects the electro-optic performances of a polymer-stabilized blue-phase or, more generally, optically isotropic LC composite. Some BPLCs are cured in an isotropic phase so that the composite is optically isotropic in the voltage-off state.[26,27] Our physical models fit experimental data well. Our general discussions apply to Kerr-effect-induced isotropic-to-anisotropic transition, regardless if it is a blue-phase or optically isotropic nanostructured composite system.

2 Brief review of Kerr effect

When a Kerr medium, such as polymer-stabilized BPLC or optically isotropic LC composite, is subject to an electric field E, the induced birefringence is related to E as[19]:

$$\Delta n_{\text{ind}} = \lambda K E^2, \tag{1}$$

where λ is the wavelength and K is the Kerr constant. From Eq. (1), the induced birefringence is linearly proportional to E^2, but this is valid only when the electric field is weak. As E keeps increasing, the induced birefringence will gradually saturate, as clearly described by the following extended Kerr effect[28]:

$$\Delta n_{\text{ind}} = \Delta n_s \left(1 - \exp[-(E/E_s)^2]\right), \tag{2}$$

where Δn_s denotes the saturated induced birefringence and E_s is the saturation electric field. In the weak-field region ($E << E_s$), we can expand Eq. (2) and deduce the Kerr constant as

$$K \approx \Delta n_s / \lambda E_s^{\,2}. \tag{3}$$

From Eq. (3), a BPLC material with high Δn_s and low E_s will result in a large Kerr constant. Roughly speaking, Δn_s governs the optical property (*e.g.,* maximum phase change) and E_s determines the electric property (operating voltage) of BPLC material. As will be discussed in detail later, the Kerr constant plays a key role in the operating voltage of BPLC devices. A typical Kerr constant for a BPLC composite is

The authors are with the College of Optics and Photonics, University of Central Florida, 4000 Central Florida Blvd., Orlando, FL 32826; telephone 407/823-6876, e-mail: lrao@ucf.edu.

about 1 nm/V^2. In 2009, Kikcuhi *et al.*[20] reported a BPLC composite with $K \sim 10$ nm/V^2 and its operating voltage in an IPS cell (5-μm electrode width and 10-μm electrode gap) is ~50 V_{rms}. In addition to material, device configuration also plays a significant role for reducing the operating voltage. With protruded IPS electrodes, Rao *et al.*[18] showed that the operating voltage could be reduced to <10 V_{rms}. This is an important milestone as the BPLC device can then be addressed by amorphous-silicon thin-film-transistors (a-Si TFTs) for achieving maximum transmittance.

Although the Kerr constant plays a crucial role in the performance of BPLC composites or optically isotropic LC composites, only scattered data are available in the literature regarding its temperature effect.[25] Moreover, the response time of these LC composites are highly sensitive to the operating temperature. In the following sections, we will present the temperature-dependent Kerr constant and response time, and then correlate these experimental results with physical models. Very good agreement between experiment and theory was found.

3 Experiment

In our experiment, the host nematic LC has a birefringence of 0.17 (λ = 589 nm, T = 20°C) and a clearing temperature of 94°C. It was mixed with chiral dopants (22.7% Merck CB15 and 4.7% ZLI-4572), monomers (3.9% RM257, 4.6% Aldrich M1, and 7.7% EHA) and a photoinitiator (1.5% darocur). The reason that we mixed some M1 is to lower the operating voltage.[29] Usually, the blue-phase temperature range is rather narrow (~3–5°C), and we need to control the cell temperature uniformly across the cell. To overcome this problem, we could conduct UV curing in an isotropic state. Similar to that cured at a blue phase, the curing in an isotropic phase also produces nanostructured optically isotropic composite, and its electro-optic properties still follow the Kerr effect. In our experiment, we filled the BPLC mixture into an IPS cell whose cell gap is 7.5 μm, the ITO (indium tin oxide) electrode width is 10 μm, and the electrode gap is 10 μm. The UV-curing process was performed at 70°C (isotropic state) for 30 min. After polymerization, the clearing temperature of the BPLC composite was measured to be T_c ~ 54°C, which was only ~5°C below that of the host LC/chiral mixture (before mixing with the monomers).

4 Results and discussion

In the following sections, we will show the measured results of the temperature-dependent Kerr constant, operating voltage, induced birefringence, and response time. The corresponding physical models and fitting results will be presented as well.

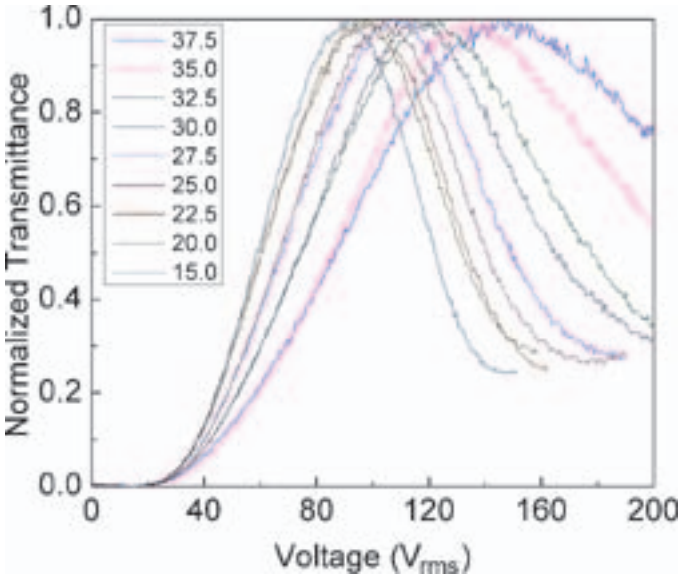

FIGURE 1 — Voltage-dependent normalized transmittance curves of the IPS LC composite cell measured from 15 to 37.5°C. Electrode width = 10 μm and electrode gap = 10 μm. λ = 441.8 nm.

4.1 Kerr constant

We first measured the voltage-dependent transmittance (VT) of our IPS cell by placing it between two crossed polarizers. A CW He–Cd laser (λ = 441.8 nm) was used as the light source. The main reason that we chose a shorter wavelength rather than a He–Ne laser (λ = 633 nm) was to obtain a transmission peak at a lower voltage. Figure 1 shows the normalized VT curves measured from 15–37.5°C (where the total phase retardation is still larger than 1π). As the temperature increases, the on-state voltage (V_{on} corresponding to the peak transmittance) shifts to the right, indicating that the Kerr constant decreases with the temperature. From Fig. 1, the on-state voltage of our BPLC sample occurs at $V_{on} \sim 90$ V_{rms} at 15°C. A high V_p implies a relatively small Kerr constant. We fitted the VT curves shown in Fig. 1 with the extended Kerr effect model [Eq. (2)] at each temperature. The obtained K values are plotted in Fig. 2. As the temperature increases, the Kerr constant decreases gradually.

To explain this trend, we need to derive the temperature-dependent Kerr constant. It has been reported by Gerber that the Kerr constant can be approximated by the following equation[30]:

$$K \sim \frac{\Delta n_{\text{ind}}}{\lambda E^2} \approx \Delta n \cdot \Delta\varepsilon \frac{\varepsilon_0 P^2}{k\lambda(2\pi)^2}. \quad (4)$$

Here, Δn_{ind} is the induced birefringence, Δn, $\Delta\varepsilon$, and k are the intrinsic birefringence, dielectric anisotropy, and elastic constant of the host LC material, respectively, and P is the pitch length. Furthermore, we know that Δn, $\Delta\varepsilon$, and k are related to the nematic order parameter (S) as $\Delta n \sim \Delta n_o S$,[31] $\Delta\varepsilon \sim S/T$, and $k \sim S^2$.[32]

Next, let us consider the temperature-dependent pitch length. If a cholesteric LC exhibits a pre-transitional

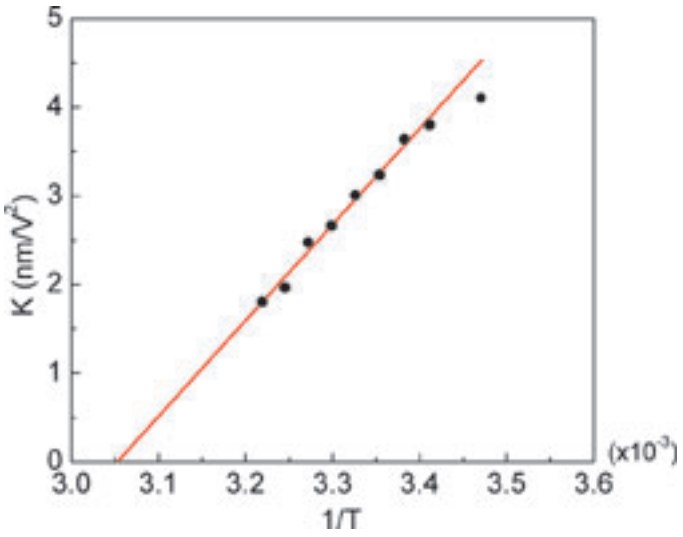

FIGURE 2 — Linear fit of the Kerr constant with the reciprocal of temperature according to Eq. (8). *T*, Kelvin temperature. The fitting parameter is $\alpha = 1.08 \times 10^{-5}$ m·*K*/*V*^{2}.

phenomenon, *e.g.*, the Smectic-A phase, then its temperature-dependent pitch length can be expressed as[33]:

$$P = Po + P_1\left(\frac{T - T^*}{T^*}\right)^{-\alpha'}, \tag{5}$$

where P_o is the cholesteric LC pitch length, T^* is the Sm-A phase-transition temperature, and P_1 and α' are fitting parameters. In the example shown in Ref. 33, $T^* \sim 297.5$ K, $P_1(1/T^*)^{-\alpha'} = 230$ nm, and $\alpha' \sim 0.78$. In the vicinity of T^*, P is indeed sensitive to the temperature. However, if the temperature is far away from T^*, *i.e.*, $T >> T^*$, then Eq. (5) can be simplified to

$$P \approx P_o + 230 \text{ nm} \cdot T^{-\alpha'}. \tag{6}$$

Under such condition, the second term in Eq. (6) is much smaller (<1%) than the first term (P_o is usually ~350 nm) and can be neglected. In our BPLC composite, although there is no Sm-A phase we can still treat T^* as a virtual transition temperature with $T >> T^*$. Thus, we can ignore the temperature effect of pitch length in Eq. (5).

Plugging these parameters into Eq. (4), we find the temperature-dependent Kerr constant has the following simple form:

$$K \approx \Delta n \cdot \Delta\varepsilon \frac{\varepsilon_o P^2}{k\lambda(2\pi)^2} \sim \Delta n_o S \cdot \frac{S}{T} \cdot \frac{1}{S^2} \cdot \frac{\varepsilon_o P^2}{\lambda(2\pi)^2} \sim \alpha \cdot \frac{1}{T}. \tag{7}$$

From Eq. (7), Kerr constant is linearly proportional to the reciprocal temperature, and α is the proportionality constant. However, as the temperature approaches the clearing point (T_c) of the LC composite, the Kerr constant should vanish (or at least dramatically decreased) because both Δn and $\Delta\varepsilon \to 0$. To satisfy this boundary condition, we rewrite Eq. (7) as follows:

$$K = \alpha \cdot \left(\frac{1}{T} - \frac{1}{T_c}\right). \tag{8}$$

Equation (8) predicts that the Kerr constant decreases linearly with reciprocal temperature (1/*T*) and eventually vanishes as the temperature reaches the clearing point of the LC composite.

To fit experimental data with Eq. (8), we treat the linear coefficient α and clearing temperature T_c as adjustable parameters. Results are depicted in Fig. 2. From fittings, we find $\alpha = 1.08 \times 10^{-5}$ $_{m \cdot K/V2}$ and $T_c = 327.58$ K (54.43°C). The obtained T_c matches very well with the measured clearing temperature (54°C) of the LC composite. Thus, Eq. (8) actually has only one adjustable parameter which is α.

In Fig. 2, as the temperature decreases (or 1/*T* increases) the Kerr constant gradually deviates from the linear extrapolation. This is because in the low-temperature region the higher-order term of the elastic constant becomes increasingly important and should be included[34]:

$$k = a_1 S^2 + a_2 S\overline{P}_4, \tag{9}$$

where a_1 and a_2 are coefficients and $\overline{P}_4$ is the fourth rank of the order parameter. From previous experimental results, in the low temperature region the second term in Eq. (9) makes ~30–40% contribution to enhance the elastic constant.[35] Thus, the Kerr constant in the low-temperature region should not increase as rapidly as the fitting line shows.

4.2 Operating voltage

Next, we study how the Kerr constant affects the on-state voltage of the IPS cell. From our previous simulation results, we found the on-state voltage is related to the Kerr constant as[18]:

$$V_{on} = A \cdot \frac{1}{\sqrt{K}}. \tag{10}$$

In Eq. (10), *A* is a device parameter; it depends on the electrode configuration. From Eq. (10), the operating voltage of a BPLC device is governed by the material (thru *K*) and device configuration (thru *A*). However, Eq. (10) has not yet been validated experimentally.

From the experimental data shown in Fig. 1, we obtain the on-state voltage at different temperatures. We then plot V_{on} against the inverse of the square root of the Kerr constant. Results are shown in Fig. 3. Indeed, a straight line passing through the origin is obtained. From the slope, we find $A = 6.07\ \mu m^{1/2}$ for our IPS structure. For the first time, the theoretical prediction of Eq. (10) is validated experimentally.

As mentioned above, the Kerr constant represents the influence from the material side to the driving voltage, while *A* represents the effect from the device design. A larger Kerr constant and smaller *A* will lead to a lower operating voltage. To illustrate the importance of the device

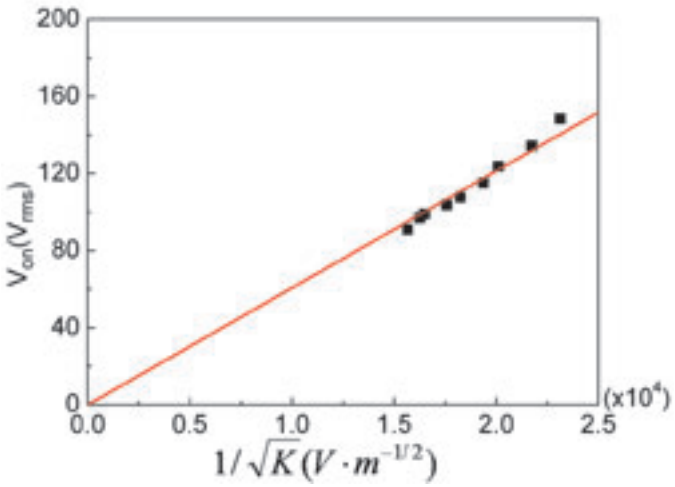

FIGURE 3 — Linear fit of V_{on} *vs.* $K^{-1/2}$ according to Eq. (10) with A = 6.07 μm$^{1/2}$.

structure, let us compare the planar IPS electrodes with protrusion electrodes. In the planar IPS structure we employed here, we have A = 6.07 μm$^{1/2}$. However, for the protrusion electrode reported in Ref. 18, it's A = 1.91 μm$^{1/2}$, which is ~3.2× smaller. As Eq. (10) shows, a small A coefficient helps to lower the operating voltage.

4.3 Temperature effect on Δn_s

From Eq. (1) and the VT curves shown in Fig. 1, we could also extrapolate the data of the saturated-induced birefringence Δn_s under different temperatures. Results are depicted in Fig. 4. As the temperature increases, Δn_s decreases gradually. To understand the responsible physical mechanisms, we need to know the temperature-dependent birefringence of the BPLC composite system.

Temperature-dependent Δn_s is proportional to order parameter (S), which in turn can be approximated by Haller's semiempirical equation[36]:

$$\Delta n_s \approx (\Delta n_s)_o S, \tag{11}$$

and

$$S = (1 - T/T_c)^{\beta}. \tag{12}$$

Here, $(\Delta n_s)_o$ is the extrapolated birefringence at T = 0K, T_c is the clearing temperature of our LC composite (~54°C), and the exponent β is a material constant. For many nematic LC materials studied, β is ~0.21 ± 0.06.[37,38] Equation (12) works well as long as the temperature is not too close (within 1°C) to the clearing point. As shown in Eqs. (11) and (12), there are two fitting parameters: $(\Delta n_s)_o$ and β. From the fitting curve shown in Fig. 4, we find $(\Delta n_s)_o$ = 0.159 and β = 0.25. We also measured the temperature-dependent birefringence of our nematic host and found $(\Delta n_s)_{o\text{-}host}$ = 0.275 and β_{host} = 0.245. The material constant β of the BPLC composite keeps almost the same as that of the host LC material. It means that the polymer only helps

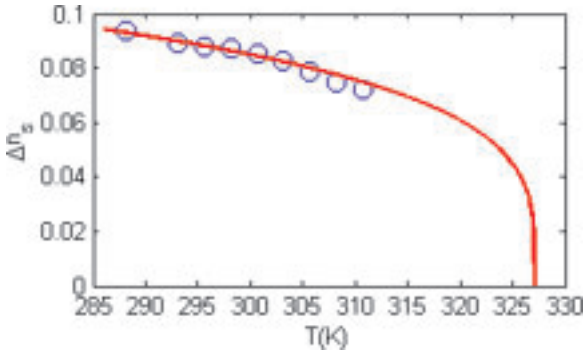

FIGURE 4 — Temperature-dependent saturated-induced birefringence. Open circles represent experimental data and line represents fitting using Eq. (11) with $(\Delta n_s)_o$ = 0.159 and β = 0.25.

to stabilize the molecular arrangement in the LC composite but does not affect the intrinsic material property of the host LC too noticeably. On the other hand, knowing $(\Delta n_s)_{o\text{-}host}$ = 0.275 and LC concentration (~54.8%) in our LC/polymer composite, we estimate that $(\Delta n_s)_o$ ~ 0.151. In comparison, through fitting our obtained $(\Delta n_s)_o$ is 0.159. The difference is less than 5%. This is another success between our experimental results and physical models.

4.4 Response time

Fast response time is one of the most attractive features of blue-phase (or optically isotropic) LCDs since it helps to reduce motion blur and enable color-sequential display while minimizing color breakup. Besides the VT curves, we also measured the decay time of our LC composite from 22.5 to 40°C. We did not measure the rise time because it depends on the applied voltage.[17] The decay time is defined as 100–10% transmittance change. The measured data are plotted in Fig. 5. As the temperature increases, the decay time decreases rapidly. For example, we note from Fig. 5 that the response time is decreased by 2× when the temperature is increased by merely 4–5°. This changing rate is ~3× more sensitive than most nematic LCs.

To understand this peculiar phenomenon, we need to develop a physical model to explicitly correlate the temperature-dependent response time with LC parameters. The free relaxation time of a polymer-stabilized blue-phase or optically isotropic LC composite can be approximated by[39,40]:

$$\tau \approx \frac{\gamma_1 P^2}{k(2\pi)^2}, \tag{13}$$

with γ_1 being the rotational viscosity, P the pitch length, and k the elastic constant. As illustrated by Eq. (6), the pitch length is insensitive to the temperature and can be treated as a constant.

From mean field theory,[32] the elastic constant is related to the nematic order parameter (S) as $k \sim S^2$. With regard to the rotational viscosity, the following modified Arrhenius

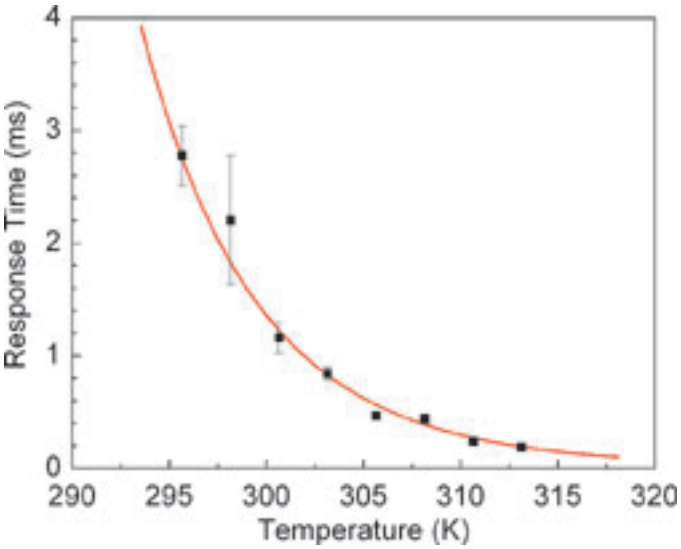

FIGURE 5 — Temperature-dependent decay time. Dots represent experimental data and line represents fitting using Eq. (15) with $B = 7.16 \times 10^{-23}$ msec and $E_a = 1.31$ eV.

model works well in describing the temperature-dependent rotational viscosity of nematic LCs[41,42]:

$$\gamma_1 \sim S \cdot \exp(E_a/K_B T), \tag{14}$$

where E_a is the activation energy of molecular rotation and K_B is the Boltzmann constant. With Eq. (14) and treating P as a constant, we can rewrite Eq. (13) as:

$$\tau \approx \frac{\gamma_1 P^2}{k(2\pi)^2} \sim \frac{S \cdot \exp(E_a/K_B T) \cdot P^2}{S^2 \cdot (2\pi)^2} \approx B \cdot \frac{\exp(E_a/K_B T)}{(1 - T/T_c)^{\beta}}. \tag{15}$$

Equation (15) has two unknowns: B and E_a. As shown in Fig. (5), Eq. (15) fits quite well with our measured response-time data. Through fitting, we obtain $B = 7.16 \cdot 10^{-23}$ msec and $E_a = 1.31$ eV. The obtained activation energy is ~3× higher than that of E7.[42,43] Our host nematic LC has a similar viscosity and E_a as E7. The increased E_a is believed to originate from the mixed chiral dopants (22.7% Merck CB15 and 4.7% ZLI-4572).

From Eq. (15), we can check how much temperature change is needed in order to result in a 2× reduction in response time. To do so, we set $\tau = \tau_1$ when $T = T_1$ and $\tau = \tau_2$ when $T = T_2$, assuming $T_2 > T_1$. Our objective is to find $(T_2 - T_1)$ which will make $\tau_2 = 0.5\tau_1$. With some algebra and assuming $\beta = 0.25$, we derive following equation:

$$T_2 - T_1 \approx 0.693 K_B T_1^2 / E_a. \tag{16}$$

Substituting $T_2 = T_1 + (T_2 - T_1)$ to the right-hand side of Eq. (16) and assuming $(T_2 - T_1) < T_1$, we find:

$$T_2 - T_1 \approx 0.693 K_B T_1^2 / E_a. \tag{17}$$

Let us assume T_1 is around room temperature (~300K) and use $E_a \sim 1.31$ eV, we find $T_2 - T_1 \sim 4$K. That is to say, the response time will decrease by 2× as the operating temperature increases by merely ~4°C. This change rate is ~3× more sensitive than E7 and MLC-6608 because our LC composite has 3× higher E_a than E7 and MLC-6608.[35]

From a response time viewpoint [Eq. (15)], a low-viscosity host (smaller activation energy) is always favorable. However, there are tradeoffs between response time and Kerr constant. For example, from Eq. (3) a smaller elastic constant leads to a larger Kerr constant, but from Eq. (13) the response time will be slower. Similarly, a larger dielectric anisotropy helps to enhance the Kerr constant, but it could dramatically increase viscosity. The polymer-stabilized blue phase or optically isotropic LC composite is a complex system, as it consists of nematic LC host, chiral agent, and two types of monomers. Material optimization and the UV-curing process all need to be optimized. This is by no means an easy task.

4.5 Remaining challenges

Although polymer-stabilized isotropic-to-anisotropic LCDs hold great potentials for future display applications, some technical challenges remain to be overcome:

(1) Low operating voltage: The protrusion electrodes substantially lower the operating voltage, but its fabrication complexity is increased. Simpler methods for reducing voltage while keeping high transmittance need to be developed.

(2) New materials: Polymer-stabilized BPLC represents a paradigm shift in materials. The conventional TFT-grade nematic LCs require a modest birefringence ($\Delta n \sim 0.1$) and dielectric anisotropy ($\Delta\varepsilon \sim 5$–10), low viscosity, and high resistivity. However, to achieve a large Kerr constant ($K \sim 10$ nm/V^2), the BPLC would need to have a high Δn (>0.2) and large $\Delta\varepsilon$ (>30). These compounds will have long molecular conjugation and large dipole moment. As a result, their viscosity will be high. Moreover, the polymer-stabilized BPLC requires two types of monomers and photo-initiator. The ionic impurities in these monomers would degrade the voltage-holding ratio. The temperature range is another concern. For display applications, the LC temperature range should cover from –40 to 80°C. In polymer-stabilized BPLC, we could choose a wide-temperature-range nematic LC host. However, after mixing with chiral dopant, the mixture's clearing point often decreases substantially. For example, the clearing temperature of our LC host is 94°C, but it drops to 54°C after polymerization. A low clearing point will make the electro-optic properties of the LC/polymer composite, *e.g.*, VT curves (Fig. 1) and response time (Fig. 5) very sensitive to the local temperature variation of a display panel. Consequently, the requirement for better thermal uniformity of a backlight unit is increased. A lot of new material development work (LC and monomers) along with the photo-polymerization process need to be studied.

(3) Hysteresis: It is known that polymer-stabilized LCs often exhibit memory effect, also known as hysteresis. Some preliminary work on the hysteresis of BPLC and poly-

mer-stabilized BPLC has been reported.[44] Hysteresis affects the accuracy of gray-scale control and should be minimized.

(4) Long-term stability: The concerns of long-term stability include twofold: incomplete photo-polymerization process and device operating lifetime, such as image sticking and polymer stability.

(5) Residual birefringence: During the polymerization process, some LC molecules could be embedded in the polymer networks. If this residual birefringence is not uniformly distributed in the entire panel, it will be difficult to be compensated by an optical film. As a result, the display contrast ratio will be degraded.

5 Conclusion

Temperature effects on polymer-stabilized blue-phase or optically isotropic liquid-crystal displays are investigated. Through the measurement of voltage-dependent transmittance under different temperatures, an analytical approximation between the Kerr constant and temperature is proposed for the first time. Moreover, the theoretical simulated relationship between the on-state voltage, Kerr constant, and device factor is experimentally validated. Finally, the temperature dependency on response time is validated through experiment and model. In all aspects, good agreement between experiment and physical model is found. These models will undoubtedly help us to optimize the device performances.

The authors would like to thank Prof. M. G. Moharam for sharing his lab equipment and ITRI (Taiwan) for financial support.

References

1 H. Hasebe and S. Kobayashi, *SID Symposium Digest* **26**, 81 (1985).
2 F. Yamada *et al., J. Soc. Info. Display* **10**, 81 (2002).
3 S. Gauza *et al., J. Display Technol.* **3**, 250 (2007).
4 F. C. Lin *et al., J. Soc. Info. Display* **17**, 221 (2009).
5 S. T. Wu and U. Efron, *Appl. Phys. Lett.* **48**, 624–626 (1986).
6 M. Jiao *et al., Appl. Phys. Lett.* **92**, 061102 (2008).
7 S. T. Wu and C. S. Wu, *J. Appl. Phys.* **65**, 527 (1989).
8 S. T. Wu, *Appl. Phys. Lett.* **57**, 986 (1990).
9 P. Bos and K. R. Koehler/Beran, *Mol. Cryst. Liq. Cryst.* **113**, 329 (1984).
10 T. Miyashita *et al., Jpn. J. Appl. Phys.* **34**, L177 (1995).
11 F. S. Y. Yeung *et al., Appl. Phys. Lett.* **88**, 041108 (2006).
12 M. Schadt, *Annual Rev. Mater. Sci.* **27**, 305 (1997).
13 H. Kikuchi *et al., Nature Mater.* **1**, 64 (2002).
14 S. W. Choi *et al., Appl. Phys. Lett.* **92**, 043119 (2008).
15 Z. Ge *et al., Appl. Phys. Lett.* **94**, 101104 (2009).
16 Z. Ge *et al., J. Display Technol.* **5**, 250 (2009).
17 K. M. Chen *et al., J. Display Technol.* **6**, 49 (2010).
18 L. Rao *et al., Appl. Phys. Lett.* **95**, 231101 (2009).
19 J. Kerr, *Philos. Mag.* **50**, 337 (1875).
20 H. Kikuchi *et al., SID Symposium Digest* **40**, 578 (2009).
21 M. Jiao *et al., Appl. Phys. Lett.* **96**, 011102 (2010).
22 S. Yoon *et al., Liq. Cryst.* **37**, 201 (2010).
23 L. Rao *et al., J. Display Technol.* **6**, 115 (2010).
24 L. Rao *et al., J. Display Technol.* **6**, 287 (2010).
25 Y. Haseba *et al., Adv. Mater.* **17**, 2311 (2005).
26 Y. Haseba and H. Kikuchi, *Mol. Cryst. Liq. Cryst.* **470**, 1 (2007).
27 Y. C. Yang *et al., SID Symposium Digest* **40**, 586 (2009).
28 J. Yan *et al., Appl. Phys. Lett.* **96**, 071105 (2010).
29 Y. H. Fan *et al., Appl. Phys. Lett.* **84**, 1233 (2004).
30 P. R. Gerber, *Mol. Cryst. Liq. Cryst.* **116**, 197 (1985).
31 S. T. Wu, *Phys. Rev. A* **33**, 1270 (1986).
32 W. Maier and A. Saupe, *Z. Naturforsch, Teil A* **15**, 287 (1960).
33 F. Zhang and D. K. Yang, *Liq. Cryst.* **29**, 1497 (2002).
34 W. M. Gelbart and A. Ben-Shaul, *J. Chem. Phys.* **77**, 916 (1982).
35 L. Rao *et al., Appl. Phys. Lett.* **94**, 071112 (2009).
36 I. Haller, *Prog. Solid State Chem.* **10**, 103 (1975).
37 S. T. Wu *et al., Appl. Opt.* **26**, 3441 (1987).
38 J. Li and S. T. Wu, *J. Appl. Phys.* **96**, 19 (2004).
39 H. F. Gleeson and H. J. Coles, *Liq. Cryst.* **5**, 917 (1989).
40 D. K. Yang and S. T. Wu, *Fundamentals of Liquid Crystal Devices* (Wiley, 2006).
41 S. T. Wu and C. S. Wu, *Liq. Cryst.* **8**, 171 (1990).
42 S. T. Wu and C. S. Wu, *Phys. Rev. A* **42**, 2219 (1990).
43 M. Schadt and F. Muller, *IEEE Trans. Electron. Dev.* ED-**25**, 1125 (1978).
44 K. M. Chen *et al., J. Display Technol.* **6**, 318 (2010).